Electrochemistry

Deutsche Ausgabe: DOI: 10.1002/ange.201606448
Internationale Ausgabe: DOI: 10.1002/anie.201606448

Magnesocene-Based Electrolytes: A New Class of Electrolytes for Magnesium Batteries

*Rainer Schwarz, Marijana Pejic, Philipp Fischer, Mario Marinaro, Ludwig Jörissen, and Mario Wachtler**

Abstract: *Unlike ferrocene, bis(η^5-cyclopentadienyl)magnesium (magnesocene, $MgCp_2$) is slightly dissociated in solvents, such as ethers, resulting in electrolyte solutions with low conductivity. $MgCp_2$/tetrahydrofuran solutions make possible reversible magnesium plating and stripping with low overpotentials for many cycles. The Mg deposits appear with a cauliflower-like morphology. IR and NMR spectroscopy confirm that the electrolyte is stable and not decomposed during prolonged cycling. The anodic stability limit is in the range of 1.5 V (at platinum) and 1.8 V versus Mg/Mg^{2+} (at stainless steel), which may be sufficient for low-voltage cathode materials. $MgCp_2$ is a first example of a completely new class of halide-free electrolytes, which may open up a new research direction for future magnesium metal and magnesium-ion batteries.*

With the advent of the digital age, the electrification of non-stationary devices puts up an ever-growing demand on energy storage—challenging today's technology. Since the end of the 20th century, lithium-ion batteries have been predominantly used in non-stationary devices. However, future needs for efficiency, capacity and availability of energy-storage solutions exceed the current state-of-the-art technology by far.[1,2]

Alternatives such as sodium- or magnesium-based secondary batteries are still in the research stage. Magnesium offers a good match to those future needs—a divalent ion with a comparatively small ionic radius of 86 pm, a feasible magnesium metal anode with a theoretical capacity of 2205 mAh g^{-1}, abundancy (magnesium is the 5th most abundant element in the earth crust) and significant commercial edge.[3,4]

Despite these promising properties, magnesium-based batteries still face major roadblocks until their commercialization. The favored, high energy density, magnesium metal anode is at the current state of research only compatible with a few different classes of magnesium salts or complexes dissolved in ethereal solution. Reversible magnesium deposition and stripping was first demonstrated in a variety of different magnesium–organic compounds, including Grignard compounds and magnesium organoborates.[5] This approach saw a great improvement in anodic stability by reacting strong chloroaluminate Lewis acids with the magnesium–organic Lewis bases.[6,7] It led to the recent development of a broad variety of different organo-halo-aluminate complexes with greatly enhanced anodic stabilities up to 3.5 V versus Mg/Mg^{2+}, lower oxygen sensitivity and low nucleophilicity,[8] as well as of inorganic chloroaluminate complexes.[9,10] Most of these electrolytes contain chlorine. It appears that they act as a source for Cl^- ions which helps to depassivate the Mg electrode and to facilitate the Mg deposition process.[11,12]

A different approach, pursuing a halide-free electrolyte, uses ethereal solutions of $Mg(BH_4)_2$,[13] the electrochemical properties of which can be further enhanced by using mixtures of $Mg(BH_4)_2$ and $LiBH_4$.[13,14] Thereupon magnesium-carboranyl salts have been developed, which exhibit an increased anodic stability of greater than 3.0 V versus Mg/Mg^{2+}.[15,16]

Conventional magnesium salts, such as halides, perhalates or imides seem to be incompatible with the magnesium metal surface.[17] As in lithium-ion batteries, the electrolyte degenerates at the surface of the magnesium metal anode. But instead of a solid electrolyte interphase with good magnesium ion conductivity a rather passivating, magnesium ion impermeable, surface layer forms, which blocks magnesium deposition. It is still under investigation if the inherent hygroscopic behavior, water content, other impurities or other properties of these conventional magnesium salts are the reason for their incompatibility with the metallic anode. Recent studies have shown that a "conditioning" of the electrolyte leads to a reaction within in the electrolyte solution, altering the electrochemical behavior and physicochemical properties, for example, solubility, of such.[18]

Here, we report a new class of halide-free electrolytes for magnesium batteries, based upon the bis(η^5-cyclopentadienyl)magnesium (magnesocene, $MgCp_2$) complex.

$MgCp_2$ was first synthesized in 1954. In its crystalline, solvent-free form the complex is built up by a magnesium ion sandwiched in between two parallel, antiprismatically staggered cyclopentadienyl rings. It is isostructural to the well-known ferrocene complex.[19,20]

In contrast to the highly stable ferrocene, $MgCp_2$ shows a very slight dissociation and ion association in solvents with electron donor properties, such as ethers [Eq. (1)].[21,22]

$$\begin{aligned} MgCp_2 &\rightleftharpoons MgCp^+ + Cp^- \\ MgCp_2 + MgCp^+ &\rightleftharpoons Mg_2Cp_3^+ \\ MgCp_2 + Cp^- &\rightleftharpoons MgCp_3^- \end{aligned} \quad (1)$$

[*] R. Schwarz, Dr. M. Pejic, P. Fischer, Dr. M. Marinaro, Dr. L. Jörissen, Dr. M. Wachtler
ZSW—Zentrum für Sonnenenergie- und Wasserstoff-Forschung Baden-Württemberg
Helmholtzstraße 8, 89081 Ulm (Germany)
E-mail: mario.wachtler@zsw-bw.de
Supporting information and the ORCID identification number(s) for the author(s) of this article can be found under http://dx.doi.org/10.1002/anie.201606448.

In tetrahydrofuran (THF) the dissociation constant of $MgCp_2$ has been determined as 1×10^{-3}.[21] $MgCp_2$ solutions exhibit a small conductivity because of this dissociative behavior. For instance, for a solution of 0.28 M $MgCp_2$ in THF a conductivity of 12.3 $\mu S\,cm^{-1}$ has been reported.[22] Although the conductivity of $MgCp_2$ and similar transition metal complexes in ethereal solutions, such as diethyl ether, THF, and 1,2-dimethoxyethane (DME), have been investigated early on,[21,22] the use of such complexes as an electrolyte salt in secondary magnesium-ion batteries has not been considered, so far.

Here, we investigate the electrochemical behavior and stability limits of a 0.5 M solution of $MgCp_2$ in THF in combination with a rechargeable magnesium metal anode.

The magnesium plating and stripping behavior in a 0.5 M solution of $MgCp_2$ in THF was investigated by extended cyclic voltammetry (CV) cycling. Figure 1a shows selected cyclic voltammograms obtained over 500 cycles at a scan rate of 10 $mV\,s^{-1}$ in a potential range of −0.5 V to 1.2 V versus Mg/Mg^{2+}.

The cathodic sweep of the first cycle shows a first reductive signal with an onset at 0.6 V versus Mg/Mg^{2+}, which is assigned to a minor side reaction. The actual magnesium deposition starts at −130 mV versus Mg/Mg^{2+}. At the cut-off potential of −0.5 V versus Mg/Mg^{2+} a current density of −0.6 $mA\,cm^{-2}$ is reached, with no indication of a limitation to the reaction. In the anodic scans no magnesium stripping overpotential is observed and a peak current density of likewise 0.6 $mA\,cm^{-2}$ is reached at a potential of 0.55 V versus Mg/Mg^{2+}. From the peak current potential to the upper cut-off potential the current decays to a residual current density of 0.03 $mA\,cm^{-2}$. It fully recedes to zero at a potential of 0.7 V versus Mg/Mg^{2+} only during the following cathodic scan, which leads to "tailing" in the cyclic voltammogram.

The deposition and stripping behavior of magnesium in this electrolyte, 0.5 M $MgCp_2$ in THF, is highly reversible resulting in outstanding cycling stability. In the 1st cycle the efficiency is 83 % because of the side reaction. Within the first five cycles it improves to approximately 97 %, to reach 98 % after 70 cycles for the remaining time of the experiment, as shown in Figure 1b.

A second set of CV experiments at a slow scan rate of 0.1 $mV\,s^{-1}$ was performed within the same potential range and in the same cell set-up. The obtained voltammogram for the first cycle is shown in Figure 2a. For the cathodic scan a lower magnesium plating overpotential of −60 mV versus Mg/Mg^{2+} is observed, and at the cut-off potential of −0.5 V versus Mg/Mg^{2+} a peak current density of 0.3 $mA\,cm^{-2}$ is reached, with

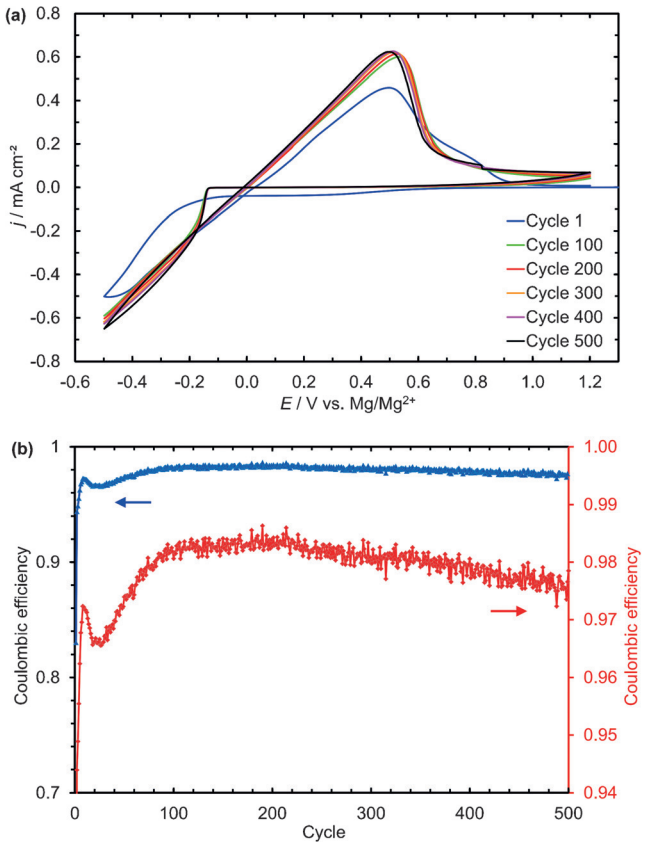

Figure 1. a) Cyclic voltammogram of the magnesium deposition and stripping reaction in a solution of 0.5 M $MgCp_2$ in THF, obtained at a scan rate of 10 $mV\,s^{-1}$ in a potential range of −0.5 V to 1.2 V versus Mg/Mg^{2+} for 500 cycles. (Working electrode: Cu, counter and reference electrodes: Mg.) b) According coulombic efficiencies for the deposition and stripping process.

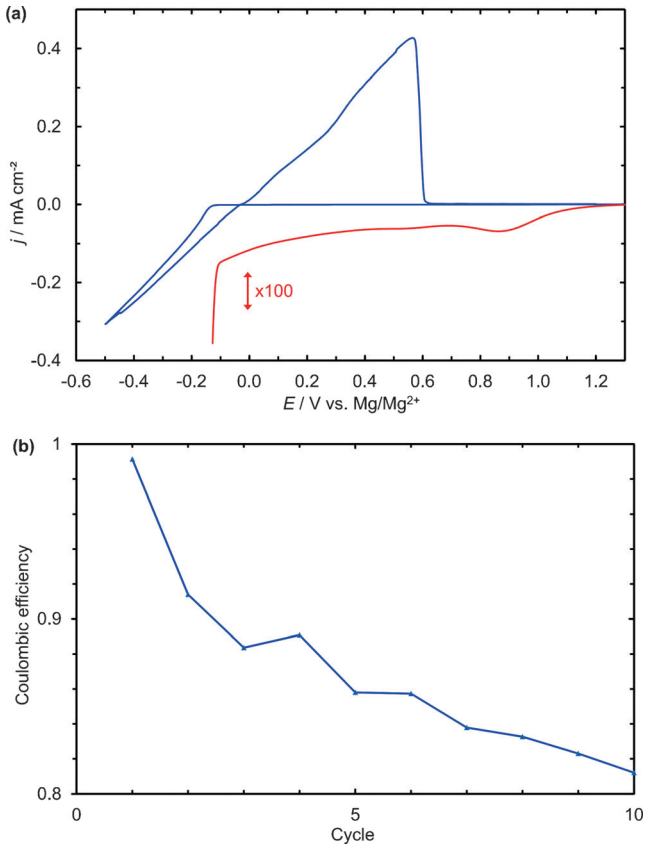

Figure 2. a) Cyclic voltammogram of the magnesium deposition and stripping reaction in a solution of 0.5 M $MgCp_2$ in THF, obtained at a scan rate of 0.1 $mV\,s^{-1}$ in a potential range of −0.5 V to 1.2 V versus Mg/Mg^{2+} for 10 cycles. (Working electrode: Cu, counter and reference electrodes: Mg.) b) According coulombic efficiencies for the deposition and stripping process.

no indication of diffusion limitation to the reaction. In the anodic scans no magnesium stripping overpotential is observed and a peak current density of 0.45 mA cm^{-2} is reached at a potential of −0.55 V versus Mg/Mg^{2+}. From the peak current potential the current decays sharply to zero at a potential of 0.62 V versus Mg/Mg^{2+}.

A third set of CV experiments at a scan rate of 5 mV s^{-1} (shown in Figure S1 in the Supporting Information) shows intermediate behavior.

Expectably, the peak current densities decline with decreasing scan rate, and the average charge throughput per cycle increases, from about 61 mC at 10 mV s^{-1} to 2.3 C at 0.1 mV s^{-1}. The minimal side reaction, which is observed in the first cathodic scan between OCV and the onset of Mg deposition for the 10 mV s^{-1} experiment, is also present in the 0.1 mV s^{-1} experiment, but only visible at proper magnification. When integrated, the reaction requires a similar amount of charge of 5.5 mC in both experiments. The irreversible capacity does hence not scale with the amount of deposited Mg or the surface of deposited Mg (which increases with the amount of deposited Mg), which could indicate, that it is either related with the reduction of surface groups of the Cu substrate or impurities in the electrolyte.

At 0.1 mV s^{-1}, the coulombic efficiency reaches 99 % in the first cycle, because of the smaller relative contribution of the side reaction (Figure 2 b). However, it decreases at higher cycle numbers to reach a value of 80 % after 10 cycles. Compared to the faster scan rate, more Mg is deposited during the experiment, and the deposited Mg particles grow bigger in size. During discharge some of the particles may lose contact to the current collector and cannot be completely dissolved any longer, which lowers the efficiency. This effect can be seen in scanning electron micrographs in Figure S4, which show two different types of Mg deposits, one with compact morphology and flat facets and another with irregular, porous (or "leached") morphology. Most likely the compact Mg represents freshly deposited material, which is in full contact with the current collector, whereas the leached Mg is a rest of a previous cycle, which lost contact during discharge and could not be completely dissolved. This effect of decreasing efficiency with decreasing scan rate (and increasing charge throughput) is not limited to the $MgCp_2$ electrolyte, but is observed for other electrolytes, such as $Mg(BH_4)_2$, as well.[23]

In comparison, the 0.5 M $MgCp_2$/THF electrolyte shows a better performance than other electrolytes, such as 0.5 M $Mg(BH_4)_2$ in THF (Figure S2) or 0.1 M $Mg(BH_4)_2$ in DME (Figure S3), when cycled in the same cell set-up and under the same conditions.

The anodic stability of the electrolyte solution was determined with linear sweep voltammetry (LSV) at various sweep rates. Figure 3 a shows the stabilities at 10 mV s^{-1} and Figure 3 b at 0.1 mV s^{-1}, respectively. The onset potentials have been determined at the point with the highest change in slope of the potential curve, which corresponds to the first maximum in the 2nd derivative of the curve.

For a scan rate of 10 mV s^{-1} the onset potentials are 1.6 V at platinum, 1.7 V at copper and 1.8 V versus Mg/Mg^{2+} at stainless steel (316 L). At a scan rate of 0.1 mV s^{-1} the onset

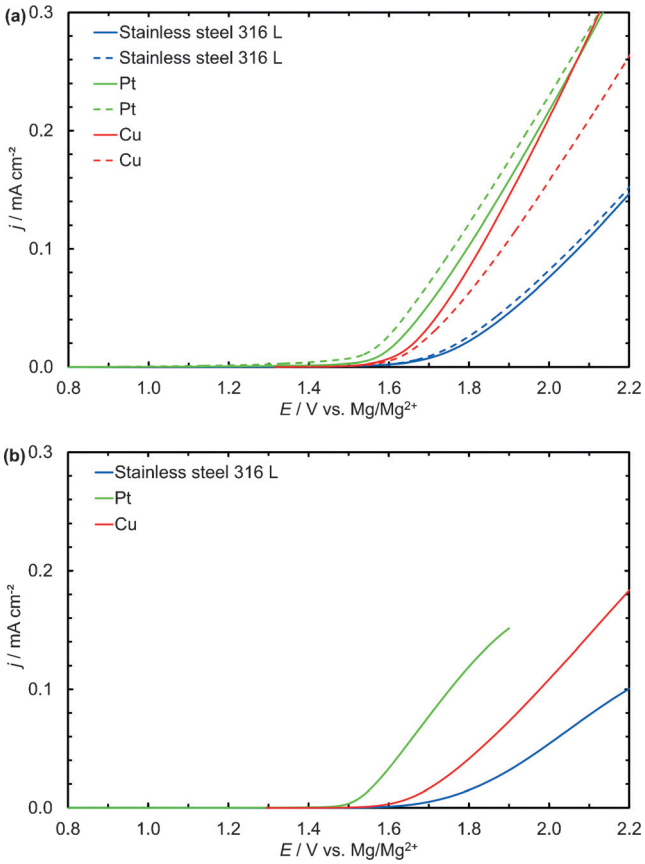

Figure 3. Linear sweep voltammogram of a solution of 0.5 M $MgCp_2$ in THF obtained at a scan rate of a) 10 mV s^{-1} and b) 0.1 mV s^{-1}. (Working electrode: Cu (red), Pt (green), stainless steel 316 L (blue), counter and reference electrodes: Mg. Dashed and solid lines: independent measurements with fresh electrodes and electrolyte.)

potentials are 1.5 V at platinum, 1.7 V at copper and 1.8 V versus Mg/Mg^{2+} at stainless steel (316 L). Therewith the oxidation stability is higher than for conventional Grignard reagents, such as n-butyl magnesium chloride (1.3 V vs. Mg/Mg^{2+} on Pt),[17] which have been investigated as electrolyte in the early stages of magnesium battery research. The CV and LSV results show that within the used potential range of 0.5 V to 1.2 V versus Mg/Mg^{2+} the electrolyte solution is fully stable. The oxidation stability of 1.5 V to 1.8 V versus Mg/Mg^{2+} offers a large enough potential window for applications in full cells with a magnesium metal anode and a Chevrel phase Mo_6S_8 cathode, working at potentials between 1.0 V and 1.6 V versus Mg/Mg^{2+}.[6] For higher voltage cathode materials, like V_2O_5,[24] the anodic stability needs to be improved. It should be mentioned that $MgCp_2$ is a nucleophile, and as such not stable in combination with cathodes such as oxygen/air or sulfur, which require non-nucleophilic electrolytes.[14,25]

The morphology and structure of the magnesium deposits have been investigated with scanning electron microscopy (SEM) and X-ray diffraction (XRD). Therefore, magnesium was deposited onto a dendritic copper foil as substrate, at a constant potential of −1.0 V versus Mg/Mg^{2+} and with a total amount of 8.25 C cm^{-2} being conducted through the cell.

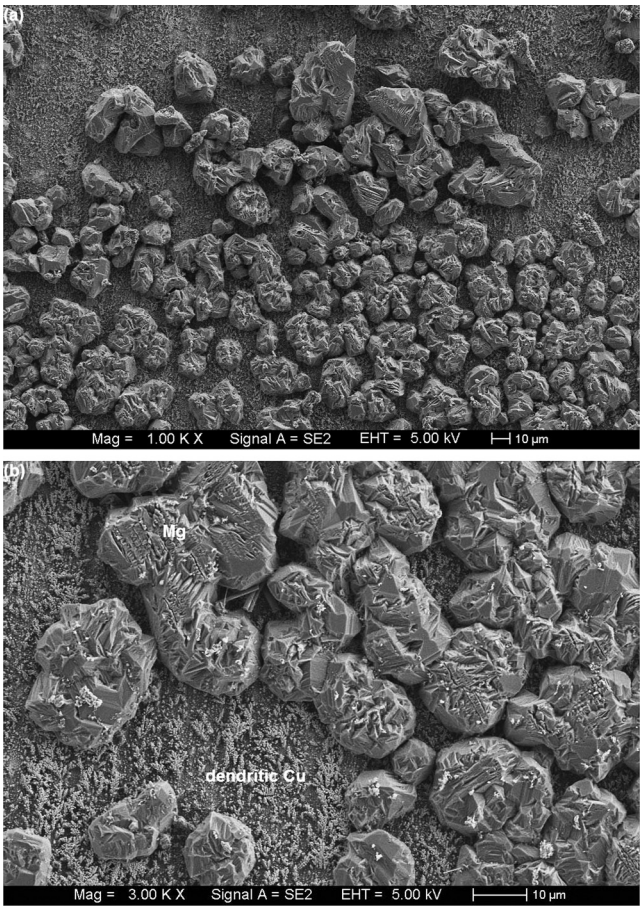

Figure 4. SEM images of magnesium plated onto a Cu working electrode at different magnifications.

As seen in Figure 4, the magnesium deposits appear in a cauliflower-like morphology, with an average particle size of 15 µm, evenly spread over the surface. The magnesium surface growth is thus less smooth and less homogenous than reported for 1M BuMgCl/THF or EtMgCl-2Me_2AlCl/THF.[7,26] However, there is no dendrite formation observed, which would pose a severe risk to safe operation through potential internal short-circuiting. A similar crystal morphology is observed after several charge/ discharge cycles, as shown in Figure S4 (Supporting Information).

The X-ray diffractogram of the magnesium deposit is shown in Figure 5. The diffraction pattern can be completely indexed to magnesium,[27] copper[28] (for the substrate) and aluminum[29] (for the sample holder). No other phases are identified. The microscopic and diffraction methods thus prove the plating of pure metallic magnesium onto the working electrode.

Attenuated total reflectance Fourier-transform infrared (ATR-FTIR) and nuclear magnetic resonance (NMR) spectroscopy results verify the electrochemical stability of the magnesocene complex and electrolyte solution during prolonged magnesium plating and stripping. The spectroscopic data and a detailed discussion are enclosed in the Supporting Information (Figures S5 and S6).

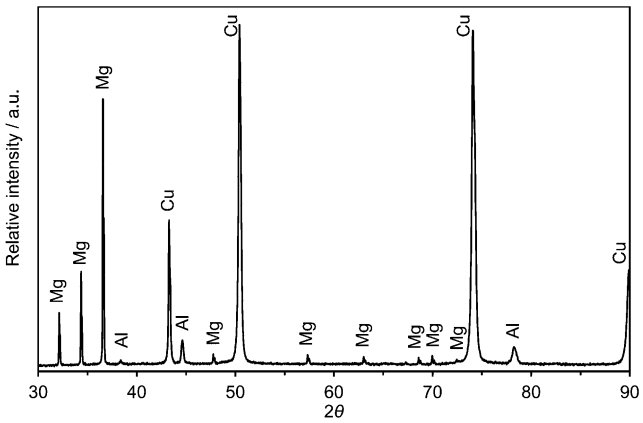

Figure 5. XRD patterns for magnesium deposited onto a copper working electrode.

The electrochemical deposition process of magnesium from 0.5M $MgCp_2$ solution in THF has been studied for the first time. The electrochemical data show, that the use of the $MgCp_2$ complex provides a highly effective electrolyte, enabling magnesium stripping and plating with minimal overpotentials, high coulombic efficiency, and excellent cycling stability. Apparently the Mg electrode is not or not strongly passivated in this type of electrolyte. The electrodeposition of magnesium was confirmed by SEM observations, which show magnesium deposits with a cauliflower-like morphology and by XRD measurements, which confirm the crystalline metallic nature of these magnesium deposits. IR and NMR spectroscopy prove the stability of the electrolyte solution upon cycling, without electrolyte degradation or changes in the electrolyte composition—at least within the detection limits of the methods.

$MgCp_2$ is a first example towards what might be a new class of halide-free magnesium electrolytes. With an anodic stability limit of approximately 1.5 to 1.8 V versus Mg/Mg^{2+} the electrochemical stability window was found to be rather narrow—large enough for low voltage cathode materials, but too narrow for higher voltage cathode materials under investigation today. However, an improvement of the anodic stability and reduction of nucleophilicity is expected for a suitable functionalization of the Cp ring, for example, with electron-withdrawing substituents and sterically hindering groups. The ionic conductivity of these aromatic sandwich complexes, acting as weak electrolytes, needs to be improved and their performance needs to be confirmed in more suitable electrolyte solvents. These studies are in progress at the moment. This new approach to Mg electrolytes may open up opportunities for future interesting developments in the field of magnesium batteries and magnesium-ion batteries.

Experimental Section

For all experiments, materials and samples were stored, handled, and prepared in an argon-filled glovebox (MBraun 200B) with oxygen and water levels below 0.5 ppm.

Materials: The solvent, THF (99.9%, inhibitor free, Sigma Aldrich), was dried with sodium and benzophenone prior to use.

The conductive salt, bis(η^5-cyclopentadienyl)magnesium ($MgCp_2$) (99.99%, ABCR), was received ampuled under argon and was used without further purification. Dendritic copper foil (99.95%, d = 0.01 mm, Schlenk), magnesium foil (99.95%, d = 0.1 mm, Gallium-Source) and magnesium wire (99.9%, d = 1 mm, Goodfellow) were used as working, counter, and reference electrodes, respectively. Prior to use, the copper foil was dried under vacuum at 120 °C and the surface of the magnesium electrodes was mechanically cleaned with a 1200-grain abrasive paper. The electrolytes were prepared by mixing the respective amounts of $MgCp_2$ and solvent inside the glovebox.

Further experimental details are included in the Supporting Information.

Acknowledgements

The authors would like to thank the German Federal Ministry of Education and Research (BMBF) for financial support within the project "Magnesium Air" (grant number 03EK3027C) and Dr. Claudia Pfeifer and Dr. Andreas Klein for their support with SEM and XRD measurements.

Keywords: electrochemistry · electrolytes · magnesium batteries · magnesocene

How to cite: *Angew. Chem. Int. Ed.* **2016**, *55*, 14958–14962
Angew. Chem. **2016**, *128*, 15182–15186

[1] K. Ozawa, *Lithium-Ion Rechargeable Batteries*, *6th ed.*, Wiley VCH, Weinheim, **2009**.
[2] R. Ruffo, S. Hong, C. Chan, R. Huggins, Y. Cui, *J. Phys. Chem. C* **2009**, *113*, 11390–11398.
[3] R. D. Shannon, *Acta Crystallogr. Sect. A* **1976**, *32*, 751–767.
[4] *CRC Handbook of Chemistry and Physics—Section 14*, *Geophysics*, *Astronomy*, *and Acoustics*; *Abundance of Elements in the Earth's Crust and in the Sea*, *85th ed.* (Ed.: D. R. Lide), CRC, Boca Raton, **2005**, p. 14.
[5] T. D. Gregory, R. J. Hoffman, R. C. Winterton, *J. Electrochem. Soc.* **1990**, *137*, 775–780.
[6] D. Aurbach, Z. Lu, A. Schechter, Y. Gofer, H. Gizbar, R. Turgeman, Y. Cohen, M. Moshkovich, E. Levi, *Nature* **2000**, *407*, 724–727.
[7] M. Matsui, *J. Power Sources* **2011**, *196*, 7048–7055.
[8] Z. R. Zhao-Karger, J. E. Mueller, X. Y. Zhao, O. Fuhr, T. Jacob, M. Fichtner, *RSC Adv.* **2014**, *4*, 26924–26927.
[9] R. E. Doe, R. Han, J. Hwang, A. J. Gmitter, I. Shterenberg, H. D. Yoo, N. Pour, D. Aurbach, *Chem. Commun.* **2014**, *50*, 243–245.
[10] T. Liu, Y. Shao, G. Li, M. Gu, J. Hu, S. Xu, Z. Nie, X. Chen, C. Wang, J. Liu, *J. Mater. Chem. A* **2014**, *2*, 3430–3438.
[11] C. J. Barile, E. C. Barile, K. R. Zavadil, R. G. Nuzzo, A. A. Gewirth, *J. Phys. Chem. C* **2014**, *118*, 27623–27630.
[12] K. A. See, K. W. Chapman, L. Y. Zhu, K. M. Wiaderek, O. J. Borkiewicz, C. J. Barile, P. J. Chupas, A. A. Gewirth, *J. Am. Chem. Soc.* **2016**, *138*, 328–337.
[13] R. Mohtadi, M. Matsui, T. S. Arthur, S.-J. Hwang, *Angew. Chem. Int. Ed.* **2012**, *51*, 9780–9783; *Angew. Chem.* **2012**, *124*, 9918–9921.
[14] Y. Shao, T. Liu, G. Li, M. Gu, Z. Nie, M. Engelhard, J. Xiao, D. Lv, C. Wang, J.-G. Zhang, J. Liu, *Sci. Rep.* **2013**, *3*, 3130.
[15] T. J. Carter, R. Mohtadi, T. S. Arthur, F. Mizuno, R. Zhang, S. Shirai, J. W. Kampf, *Angew. Chem. Int. Ed.* **2014**, *53*, 3173–3177; *Angew. Chem.* **2014**, *126*, 3237–3241.
[16] O. Tutusaus, R. Mohtadi, T. S. Arthur, F. Mizuno, E. G. Nelson, Y. V. Sevryugina, *Angew. Chem. Int. Ed.* **2015**, *54*, 7900–7904; *Angew. Chem.* **2015**, *127*, 8011–8015.
[17] O. Tutusaus, R. Mohtadi, *ChemElectroChem* **2015**, *2*, 51–57.
[18] I. Shterenberg, M. Salama, H. D. Yoo, Y. Gofer, J.-B. Park, Y.-K. Sun, D. Aurbach, *J. Electrochem. Soc.* **2015**, *162*, A7118–A7128.
[19] E. O. Fischer, W. Hafner, *Z. Naturforsch. B* **1954**, *9*, 503.
[20] G. Wilkenson, F. A. Cotton, *Chem. Ind.* **1954**, 307.
[21] W. Strohmeier, H. Landsfeld, F. Cernert, *Z. Elektrochem.* **1962**, *66*, 823–827.
[22] W. Strohmeier, F. Seifert, H. Landsfeld, *Z. Elektrochem.* **1962**, *66*, 312–316.
[23] R. Schwarz, et al., unpublished results.
[24] D. Imamura, M. Miyayama, *Solid State Ionics* **2003**, *161*, 173–180.
[25] Z. R. Zhao-Karger, X. Y. Zhao, D. Wang, T. Diemant, R. J. Behm, M. Fichtner, *Adv. Energy Mater.* **2015**, *5*, 1401155.
[26] D. Aurbach, I. Weissman, Y. Gofer, E. Levi, *Chem. Rec.* **2003**, *3*, 61–73.
[27] H. E. Swanson, E. Tatge, *Natl. Bur. Stand. Rep.* **1953** (ICDD PDF No. 00-004-0770).
[28] S. Srinivasa-Rao, T. R. Anantharaman, *Curr. Sci.* **1963**, *32*, 262 (ICDD PDF No. 01-070-3038).
[29] P. D. Wheeler, *Phys. Rev.* **1925**, *25*, 753 (ICDD PDF No. 00-001-1176).

Received: July 3, 2016
Revised: September 20, 2016
Published online: October 28, 2016

